STRESS CHANGE HISTORY OF THE 2000 TOTTORI-KEN-SEIBU EARTHQUAKE

Hisashi TANIYAMA
Vibration Engineering Lab., Department of Civil and Environmental Engineering, Saitama University

ABSTRACT

The stress change history of the 2000 Tottori-ken-seibu earthquake is determined using the strong motion records. To express a spatiotemporal stress distribution on the fault, the fault plane is divided into subfaults and the shear stress on a subfault after the passage of the rupture front is assumed to change repeatedly to its residual stress. Stress changes of subfaults are inferred directly from the observed ground motions. The result shows large stress drop in the upper central part of the fault. Negative stress drop is observed at the NW and SE sides of the fault at the depths between 5 and 10 km. The slip distributions agree with those obtained from kinematic models. The stress-time histories in the high stress drop zones show predominantly monotonic stress drop.

KEYWORDS: 2000 Tottori-ken-seibu earthquake, Strong ground motion, Inversion

1. INTRODUCTION

Detailed information about dynamic rupture processes of large earthquakes is significant for the precise prediction of strong ground motions. Kinematic inversion analyses have been carried out to obtain spatiotemporal slip distributions, from which the stress distributions and the constitutive relation between slip and stress on the fault plane have been inferred (e.g., Quin, 1990, Miyatake, 1992, Fukuyama and Mikumo, 1993, Ide and Takeo, 1997, Day et. al., 1998, Mikumo et. al., 2003).

In kinematic waveform inversions, a fault is usually divided into subfaults and time histories of displacement on subfaults are inferred. With a proper modification, the method used in kinematic waveform inversions can be used to infer a spatiotemporal stress distribution from observed waveforms.

In this study, an inversion method to infer stress drop process of an earthquake fault is developed to determine the stress change history of the 2000 Tottori-ken Seibu earthquake.

2. METHOD

2.1 Stress distribution on a fault plane

To express a stress change history, the shear stress at a point on a fault surface after the passage of the rupture front is assumed to change repeatedly to its residual stress (Fig. 1). In linear elastodynamics, seismic waves are sensitive to stress change and insensitive to absolute stress level. Thus in this study, only stress changes are dealt with, i.e., we assume τ_0 (initial stress) = 0. Accordingly the displacement is measured from the state at $t = 0$.

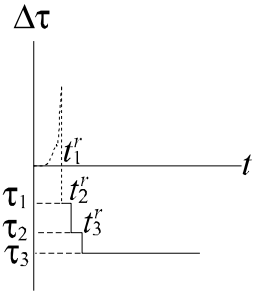

Figure 1. Assumed stress change history.

Shear stress before the rupture is calculated based on the theory of linear elasticity. This stress change history is expressed as

$$\Delta\tau = \mu\left(\frac{\partial u_s}{\partial x_n} + \frac{\partial u_n}{\partial x_s}\right) \quad (\text{if } t < t_1^r) \tag{1}$$

and

$$\phi(t) = \tau_k \quad (t_k^r \le t < t_{k+1}^r) \tag{2}$$

where t_1^r is the time of the passage of the rupture front, μ is the Lamé modulus. 'n' indicates the direction normal to the fault plane. The shear stress considered in Eq. (1) and Eq. (2) is assumed to act

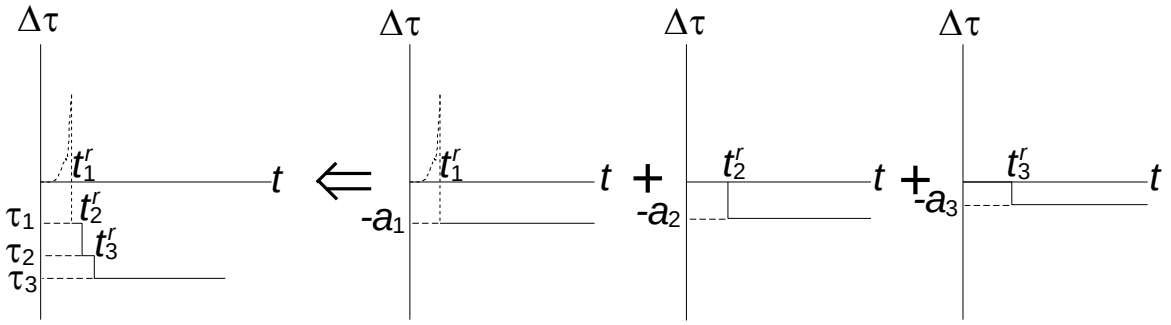

Figure 2. Division of the stress drop process.

in the direction of 's'. $\phi(t)$ in Eq. (2) is a function of time that satisfies the following equation

$$\phi(t) = \tau_k \quad (t_k^r \le t < t_{k+1}^r) \tag{3}$$

where t_k^r is the time when the *k*th stress change occurs.

As shown in Fig. 2, $\phi(t)$ can be expressed as the sum of the functions $\varphi_k(t)$, representing unit stress drop at $t = t_k^r$.

$$\phi(t) = \sum_{k=1}^{K} a_k \varphi_k(t) \tag{4}$$

where *K* is the total number of stress changes. The expansion coefficients a_k in Eq. (4) indicate the stress change at $t = t_k^r$ and are given by

$$a_1 = -\tau_1 \tag{5}$$

$$a_k = \tau_{k-1} - \tau_k \quad (k \ge 2) \tag{6}$$

To infer a spatial distribution of stress, a fault is divided into subfaults. If each subfault is expressed as a crack on which the stress drop occurs, the displacement at the edge of the subfault is 0 and the stress near the tip of the subfault becomes high. If we sum up these displacements and stresses, the resultant displacement and stress distribution may be different from the one on the actual fault surface. Therefore, the following conditions are imposed on the assumed fault and subfaults.

$$\Delta\tau(\xi) = \mu\left(\frac{\partial u_s}{\partial x_n} + \frac{\partial u_n}{\partial x_s}\right) \quad (\text{if } t < t_1^r(\xi)) \tag{7}$$

$$\Delta\tau(\xi) = \varphi_k(t, \xi)$$

(if $t \ge t_1^r(\xi)$ and ξ is on the subfault) (8)

$$\Delta\tau = 0$$

(if $t \ge t_1^r(\xi)$ and ξ is outside the subfault but on the fault plane) (9)

where ξ is a point on the fault surface.

2.2 Inversion method

Once we calculate the waveform ($u_{ijk}(t)$) at the *i*th station generated by $\varphi_{jk}(t)$ (i.e., unit stress drop on the *j*th subfault at $t = t_k^r$ hen the *i*th synthetic seismogram $u_i(t)$ is given by the summation of $u_{ijk}(t)$ multiplied by the stress drop (a_{jk}) on the *j*th subfault at $t = t_k^r$

$$u_i(t) = \sum_{j,k} a_{jk} u_{ijk}(t) \tag{10}$$

The *i*th observed record is expressed by the discrete time series of $O_i(t_l)$, l=1, *L*, where *L* is the total number of time points for the record. The equation with observed waveform $O_i(t_l)$ is expressed as

$$O_i(t_l) = u_i(t_l) + e_i(t_l) = \sum_{jk} a_{jk} u_{ijk}(t_l) + e_i(t_l) \tag{11}$$

where $e_i(t_l)$ is the error between the observed and synthetic seismogram. a_{jk}, j=1,*J* and k=1,*K* are the model parameters to be determined. Here *J* is the total number of subfaults. In inferring the model parameters a_{jk}, along with Eq. (11), smoothing constraints are added to reduce instability and repress excessive variances in model parameters. Based on the presumption that stress changes close together in space and in time should be similar, two constraints (i.e., the temporal constraint and the spatial constraint) are assigned. In addition to the above smoothing constraints, the condition that final displacements on all subfaults are nonnegative is imposed. Parameters that minimize the error in Eq. (11) and in the smoothing constraints satisfying the nonnegative condition are inferred by least squares (Lawson and Hanson,

1995). The optimal values of hyperparameters that control the strength of the smoothing constraints are determined objectively based on Akaike's Bayesian information criterion (ABIC) (Akaike, 1980, Yabuki and Matsu'ura, 1992, Ide and Takeo, 1997).

3. ANALYSIS OF THE 2000 TOTTORI-KEN SEIBU EARTHQUAKE

A strong earthquake measuring 7.3 in magnitude (M_{JMA}) occurred at 13:30 October 6 2000. The epicenter was in the west part of Tottori, Japan. Using the observed seismograms, stress changes on the fault plane are determined by the method described in the previous chapter.

3.1 Model

Ground motion records observed at K-NET stations and KiK-net stations are used in the analysis. Observed accelerometer data are integrated to velocity and are 0.1Hz-1.0Hz bandpass filtered.

We assume a vertical fault plane striking at 150 °NE and that the shallowest edge of the fault is 1km. Fig. 3 shows the location of the stations, the epicenter of the earthquake and the assumed fault line.

The following equations were solved by finite difference method (Virieux and Madariaga, 1982).

$$\rho \dot{v}_i = \sigma_{ij,j} \tag{12}$$

$$\dot{\sigma}_{ij} = \lambda v_{k,k}\delta_{ij} + \mu\left(v_{i,j} + v_{j,i}\right) \tag{13}$$

where ρ is the density of the medium, σ_{ij} is the ij component of the (incremental) stress, λ and μ are the Lamé moduli, v_k is the k component of the velocity and δ_{ij} is Kröncher's delta. Dots indicate time derivatives, commas partial differentiation with respect to the space component indicated by the index following comma. The intervals of the staggered grids and time are 250 m and 0.01 s respectively. Assumed density, P-wave and S-wave velocity are listed in Table 1.

The length and the width of the fault are assumed 22.5km and 13.5km, respectively. The fault is divided into sixty 2.25km ×2.25km subfaults (10 in strike direction and 6 in vertical direction). We assume the hypocenter is located at the depth of 7.8km, 35.269N and 133.3567E and that the rupture front propagates at the velocity of 1.9km/s. Waveforms at the stations due to the stress change on each subfault are calculated and used in the inversion analysis. The shear stress on each subfault is assumed to change when the rupture front passes and also at 0.4s, 0.8s, … , 2.8s after the passage of the rupture front (8 times in total at the interval of 0.4s).

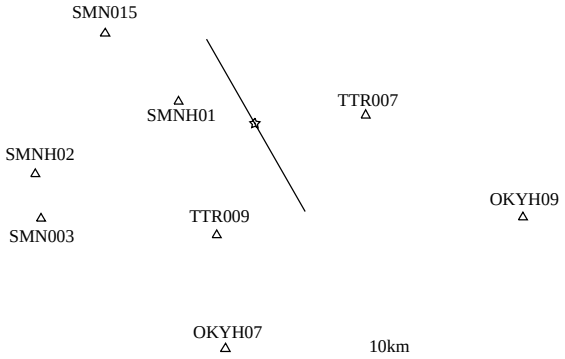

Figure 3. Location of the stations (triangle), the epicenter (star) and the assumed fault line.

Table 1. P-wave and S-wave velocity and density of the model

Depth	P-wave velocity	S-wave velocity	Density
0km	5.5km/s	3.18km/s	2.6g/cm^3
2km	6.1km/s	3.53km/s	2.7g/cm^3
16km	6.7km/s	3.87km/s	2.8g/cm^3

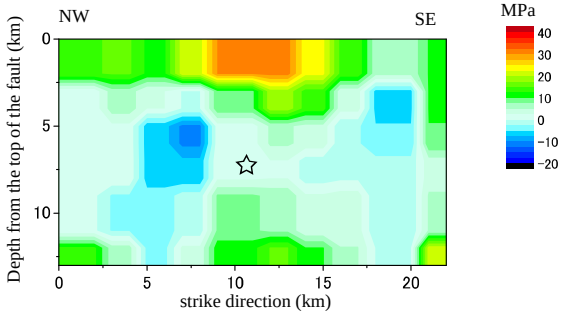

(a) strike direction

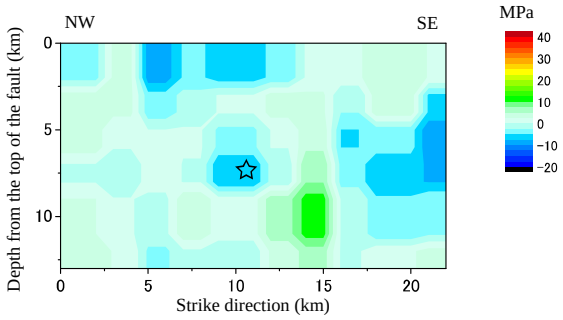

(b) vertical direction

Figure 4. Inferred stress change distribution

3.2 Result

Fig. 4 shows the inferred stress change distribution. Stress at each grid point of the FDM analysis at the end of the analysis (10s after the rupture starts) is shown. In Fig. 4 (a), shear stress in the strike direction is shown (positive in the case of stress drop) and in Fig. 4 (b) shear stress in the

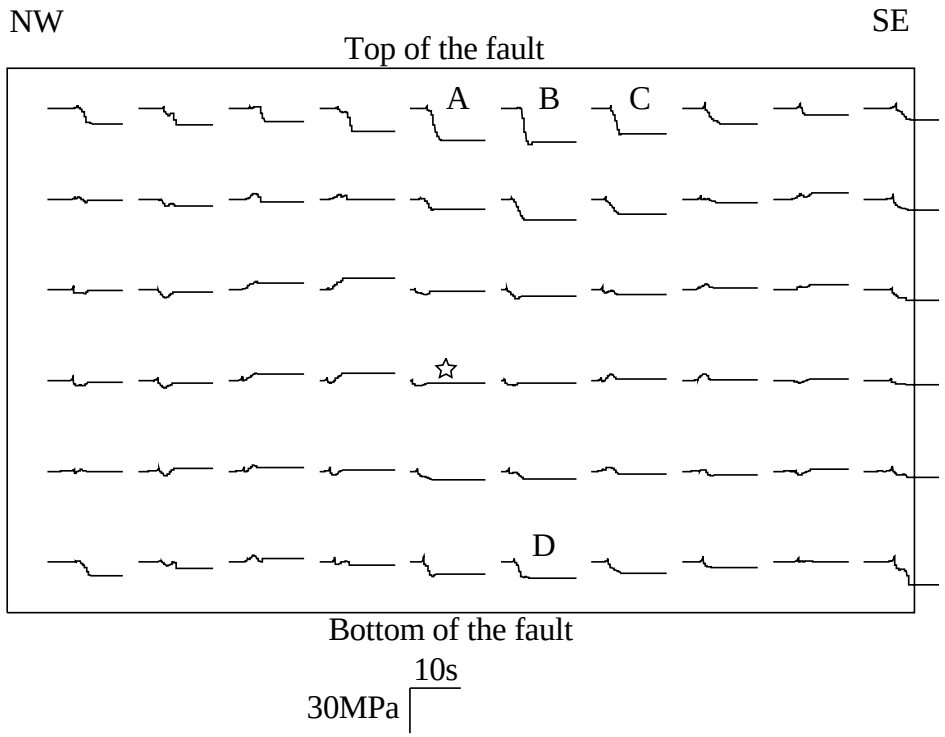

Figure 5. Inferred time histories of shear stress change on the fault plane. The left edge of each curve is positioned at the fault plane point to which it is corresponds.

vertical direction is shown (positive if NE side moves upward with respect to SW side).

Stress change in the strike direction is dominant, and large stress drop is observed in the upper central part of the fault and relatively large stress drop in the center deep part of the fault. Stress change of about 15 MPa occurs in some parts of the fault in the vertical direction, but these stress changes are small in value and area compared to the stress change in the strike direction.

The inferred shear stress change, as a function of time, is shown in Fig. 5. The stress-change time history at the center of each subfault is shown, with the location of the left edge of each curve indicating the location of the point. Because stress change in the strike direction is dominant, only stress-change history in the strike direction is shown (positive up).

Fig. 6 compares the observed and synthetic wave form.

Stress drops at and around the hypocenter as the rupture starts but the stress drop in these areas is small. Large stress drop occurs at the upper central part of the fault (A, B and C in Fig. 5) around 4-5s. Most of the stress drop in these areas occurs within 3-4 steps of stress change (0.8 s to 1.2 s duration) and the stress change is mainly monotonic stress drop with no or little restrengthening observed. Large stress drop in deep part of the fault (D in Fig. 5) also occurs around 4-5s and within 4-5 steps of stress change (1.2 s to 1.6 s duration).

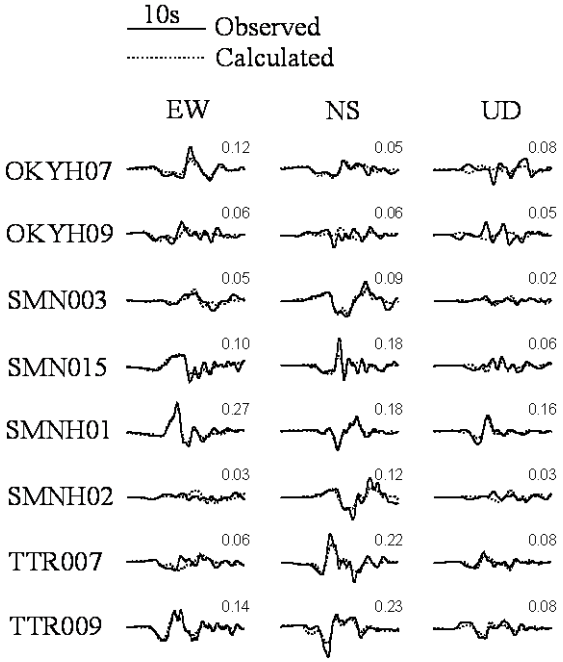

Figure 6. Comparison of observed and synthetic wave form.

Due to the smoothing and bad resolution in the deep part of the fault, it is probable that this duration is overestimated. In other areas of shallow

part of the fault and some areas of deep part of the fault, relatively large stress drop is observed, but except these areas stress drop is small and negative stress drop is observed at the NW and SE sides of the fault at the depths between 5 and 10 km.

3.3 Comparison with kinematic results

Slip distribution on the fault plane is calculated using the inferred stress change distribution (Fig. 7). The figure shows the move of the NE block with respect to the SW block.

Horizontal slip is large compared with vertical slip. Slip in the shallow part of the fault is large and the maximum slip of about 4 m is observed at the center shallow part of the fault. In other part of the fault (deeper than 5 km from the top of the fault), slip is small and slip of about 1m is observed in areas from the hypocenter to about 5 km SE along the strike. The slip distribution corresponds to the stress change distribution in that stress drop in the strike direction is large and that stress drop in deep part of the fault is generally small.

The slip distribution inferred by kinematic inversion (Iwata and Sekiguchi, 2002) shows that large slip is located from the hypocenter to about 8km SE along the strike in the shallow part of the fault and that maximums slip is about 4m. Slip in deep part of the fault is small. Although there are differences in that larger slip is observed around the hypocenter in Fig. 7, overall slip distribution pattern is similar between the two results.

The dynamic and static stress changes (Dauguer et.al., 2002) recovered from the kinematic inversion result (Iwata and Sekiguchi, 2002) show an asperity zone in the upper central part of the fault. The maximum stress drop of the asperity zone is 30 MPa. Relatively large stress drop (about 10 MPa) is observed in the area 5 km to 10 km SE from the hypocenter at depths between 2 km and 12 km. Although small stress drop is observed in NW part of the fault, there are similarities between the two models such as the location of asperity and maximum stress drop.

It is shown that the inversion method developed in this study gives similar slip and stress-change distribution as the kinematic inversion if the same data are used. If a slip-time function based on the stress change is used, kinematic inversion gives slip distribution based on the stress change process. But in calculating the slip-time function, rise time is needed. Rise time depends on the size of asperity zone and is difficult to determine before the inversion analysis. The inversion method developed in this study does not need rise time. The effect of the stress change of a subfault on other subfaults is also considered. If a lot of nearfield data are available, the inversion method developed in this study has an advantage that it can directly infer stress change from the observed data.

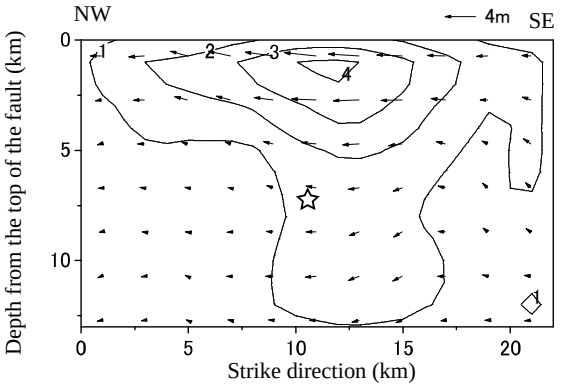

Figure 7. Slip distribution

4. CONCLUSION

The stress change history of the 2000 Tottori-ken-seibu earthquake is determined using the strong motion records. The fault plane is divided into subfaults and the shear stress changes on subfaults are inferred directly from the observed ground motions. The result shows large stress drop in the upper central part of the fault. Negative stress drop is observed at the NW and SE sides of the fault at the depths between 5 and 10 km. The slip distributions agree with those obtained from kinematic models. The stress-time histories in the high stress drop zones show predominantly monotonic stress drop

5. ACKNOWLEDGEMENT

We thank National Research Institute for Earth Science and Disaster Prevention for the use of K-NET and Kik-net data.

6. REFERENCES

Akaike H., (1980) “Likelihood and the Bayes procedure”, Bayesian Statistics (Bernardo J. M., De Groot M. H., Lindley D. V. and Smith A. F. M., eds.), University Press, Valencia, Spain, pp. 143-166.

Dalguer, L. A. et al. (2002) “Distribution of dynamic and static stress changes during 2000 Tottori (Japan) earthquake: Brief interpretation of the earthquake sequences; foreshocks, mainshock and aftershocks”, Geophys. Res. Letters, Vol. 29, No. 16, 1758, doi:10.1029/2001GL014333.

Day S. M., Yu G. and Wald D. J., (1998) “Dynamic stress changes during earthquake rupture”, Bull. Seism. Soc. Am., Vol. 88, No. 2: pp. 512-522.

Fukuyama E. and Mikumo T., (1993) “Dynamic rupture analysis: Inversion for the source process of the 1990 Izu-Oshima Japan earthquake (M=6.5)”, J. Geophys. Res., Vol. 98, No. B4: pp. 6529-6542.

Ide S. and Takeo M., (1997) “Determination of constitutive relation of fault slip based on seismic wave analysis”, J. Geophys. Res., 102: pp. 27379-27391.

Lawson C. L. and Hanson R. J., (1995) “Solving least squares problems” SIAM, (an unabridged, revised republication of the work first published by Prentice-Hall, 1974)

Miyatake T., (1992) “Reconstruction of dynamic rupture process of an earthquake with constraints of kinematic parameters”, Geophys. Res. Lett., Vol.19, No.4: pp. 349-352.

Mikumo T., Olsen K. B., Fukuyama E. and Yagi Y., (2003) “Stress-breakdown time and slip-weakening distance inferred from slip-velocity functions on earthquake faults”, Bull. Seism. Soc. Am., Vol. 93, No. 1: pp. 264-282.

Quin H., (1990) “Dynamic stress drop and rupture dynamics of the October 15 1979 Imperial valley California earthquake”, Tectonophysics, 175: pp. 93-117.

Virieux, J. and Madariaga R., (1982) “Dynamic faulting studied by a finite difference method”, Bull. Seism. Soc. Am., 72: pp. 345-369.

Yabuki T. and Matsu'ura M., (1992) “Geodetic data inversion using a Bayesian information criterion for spatial distribution of fault slip”, Geophys. J. Int., 109: pp. 363-375.